BASIC SCIENCE

Nanomedicine: Nanotechnology, Biology, and Medicine
7 (2011) 992–1000

Research Article

nanomedjournal.com

Design and potential application of PEGylated gold nanoparticles with size-dependent permeation through brain microvasculature

Arnold B. Etame, MD[a], Christian A. Smith, PhD[a], Warren C.W. Chan, PhD[b], James T. Rutka, MD, PhD[a,*]

[a]*The Hospital for Sick Children, University of Toronto, Toronto, Ontario, Canada*
[b]*Department of Materials Science and Engineering, University of Toronto, Toronto, Ontario, Canada*

Received 22 November 2010; accepted 14 April 2011

Abstract

Gold nanoparticles (AuNPs) have gained prominence in several targeting applications involving systemic cancers. Their enhanced permeation and retention within permissive tumor microvasculature provides a selective advantage for targeting. Malignant brain tumors also exhibit transport-permissive microvasculature secondary to blood-brain barrier disruption. Hence AuNPs may have potential relevance for brain tumor targeting. However, there are currently no studies that systematically examine brain microvasculature permeation of polyethylene glycol (PEG)-functionalized AuNPs. Such studies could pave the way for rationale AuNP design for passive targeting of malignant tumors. In this report we designed and characterized AuNPs with varying core particle sizes (4–24 nm) and PEG chain lengths [molecular weight 1000–10,000]. Using an in-vitro model designed to mimic the transport-permissive brain microvasculature, we demonstrate size-dependent permeation properties with respect to core particle size and PEG chain length. In general short PEG chain length (molecular weight 1000–2000) in combination with smallest core size led to optimum permeation in our model system.

From the Clinical Editor: In this report the authors designed and characterized PEGylated gold NPs with varying core particle sizes and PEG chain lengths and demonstrate that short PEG chain length in combination with smallest core size led to optimum permeation of a blood-brain barrier model system. These findings may pave the way to optimized therapy of malignant brain tumors.

Key words: Polyethylene glycol; Gold nanoparticles; Permeation; Brain microvasculature; Brain tumors

Advances in nanotechnology have significant implications in oncology with respect to diagnostic and therapeutic delivery applications. In particular, nanotechnology-based delivery systems provide a novel avenue for targeting malignant brain tumors where the current prognosis is dismal, by circumventing some of the challenges associated with conventional therapy. Within the context of tumor targeting, nanoparticles (NPs) must traverse the porous tumor vasculature so as to deliver their payload onto tumor cells. The unique ability of NPs and other macromolecules to permeate and accumulate within tumors has been defined as enhanced permeability and retention (EPR).[1,2] EPR serves as a selective modality for passive targeting of tumors whereby the porous tumor microvasculature allows for permeation and retention of NPs.[1,2] Similar to their systemic counterparts, malignant brain tumors demonstrate alterations of blood-brain barrier integrity resulting in a transport-permissive microvasculature.[3-7] Hence NP-mediated strategies in systemic cancers may have potential relevance in malignant brain tumor targeting. Ultimately, the design features as well as core composition of the NP will hypothetically have a significant bearing on the NP permeation and effectively targeting within compromised brain tumor microvasculature.

Inert and nonimmunogenic NPs such as gold nanoparticles (AuNPs)[8,9] have gained prominence in nano-mediated cancer targeting. Several tumor-targeting[10-13] as well as photothermal cancer therapy[14-19] applications have been demonstrated for AuNPs as well. Moreover, there are several polyethylene glycol (PEG)-formulated anticancer AuNP targeting agents currently in clinical trial with promising phase I data.[20] The successful extrapolation and application of AuNP anticancer therapy to the malignant brain tumors will ultimately require an improved understanding of AuNP permeation through the brain

We acknowledge the Canadian Institute of Health Research, Penfield Fellowship Award from the Congress of Neurological Surgeons, Brain Tumour Foundation of Canada, and Brainchild for financial support.

*Corresponding author: The Arthur and Sonia Labatt Brain Tumor Research Centre, The Hospital for Sick Children, Department of Neurosurgery, University of Toronto, Toronto M5S 3G9, Ontario Canada.

E-mail address: james.rutka@sickkids.ca (J.T. Rutka).

1549-9634/$ – see front matter © 2011 Elsevier Inc. All rights reserved.
doi:10.1016/j.nano.2011.04.004

Please cite this article as: A.B. Etame, C.A. Smith, W.C.W. Chan, J.T. Rutka, Design and potential application of PEGylated gold nanoparticles with size-dependent permeation through brain microvasculature. *Nanomedicine: NBM* 2011;7:992-1000, doi:10.1016/j.nano.2011.04.004

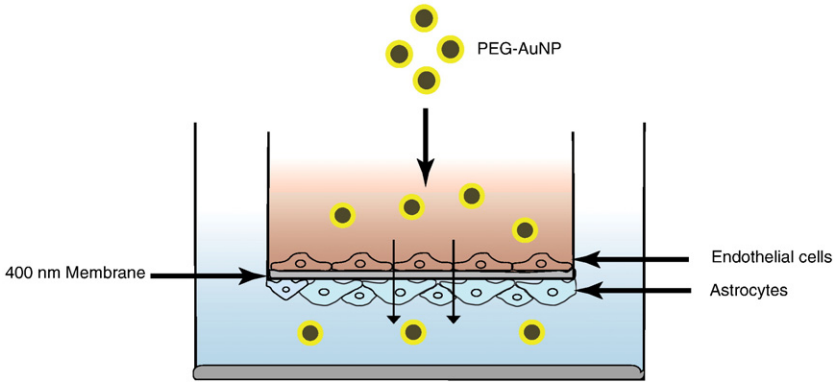

Figure 1. Experimental scheme with Transwell double chamber co-culture system of rat brain endothelial cells (RBECs) and rat astrocytes (RAs) designed for assessing microvasculature transport of PEG-AuNPs. The co-culture system, which is designed to mimic the transport-permissive brain microvasculature, consists of an upper and lower chamber separated by a 400-nm microporous membrane. RBECs are seeded on the upper surface of the membrane, and RAs are seeded on the bottom surface of the membrane. When cells are completely confluent for a couple of days, PEG-AuNPs are introduced into the upper endothelial chamber. At fixed time points, the medium of both chambers is quantitatively analyzed for gold content by inductively coupled plasma-atomic emission spectrometry.

microvasculature. Yet there are currently no studies that have systematically assessed the permeation of PEG-AuNPs through permissive-transport brain microvasculature. Such information could lead to optimization of permeation design parameters necessary for effective delivery of therapeutics to malignant brain tumors with permissive microvasculature. Given that AuNPs are readily amenable to size-dependent synthesis and surface polymeric modifications, they serve as an ideal nanocarrier system for studying physical design influences on permeation.

Consequently, given that AuNPs have generated a lot of interest because of their tumor-targeting potential for systemic cancers, it was deemed important to ascertain the permeation profile of AuNPs within the brain microvasculature for subsequent malignant brain tumor applications. Therefore, the present study focused on the design of AuNPs with various PEG chain sizes, and subsequent assessment of their size-dependent permeation through an in vitro model of a transport-permissive rat brain microvasculature. Moreover, surface polymeric formulations such as PEG confer several advantages, including stability, biocompatibility, and multifunctionality.[21-26]

Hence this study was undertaken to characterize permeation of AuNPs through an in vitro platform designed to mimic the brain microvasculature. Prior observations in a flank model of a breast tumor by one of the co-authors suggested a size-dependent permeation profile of PEG-functionalized AuNPs (PEG-AuNPs).[27] In that study an inverse correlation was noted between permeation and retention. The smaller particles had the fastest permeation kinetics and were less likely to be retained within the tumor as compared to larger particles. Based on those observations, we hypothesized that a similar size-dependent phenomenon would be observed if brain microvasculature endothelial cells were permissive to PEG-AuNP permeation. More importantly, we sought to evaluate the permeation effects of PEG-chain polymeric design.

To test this hypothesis in vitro, we employed a co-culture system of fully confluent rat brain endothelial cells (RBECs) and rat astrocytes (RAs) designed to mimic the blood-brain interface. Given that the assessment of permissive transport was the goal of our study, we employed a range of AuNPs that encompassed various sizes that have previously been reported to traverse the blood-brain interface following in vivo biodistribution.[28,29] We demonstrate size-dependent permeation of PEG-AuNPs with the smallest NPs exhibiting the greatest permeation. Furthermore, we demonstrate that PEG surface polymeric chain was a critical permeation determinant for the smaller NPs when compared to larger NPs within our range.

Methods

Materials and methods, cell culture

RBECs (Cell Applications, San Diego, California) were maintained in RBEC growth medium (Cell Applications) supplemented with 1% (vol/vol) penicillin/streptomycin (Wisent Inc., St. Bruno, Quebec, Canada) and grown in dishes coated with a type IV collagen attachment factor (Cell Applications). RAs (ScienCell, Carlsbad, California) were maintained in supplemented RA growth medium (ScienCell). Cultures were incubated at 37°C in an atmosphere with 5% CO_2.

AuNP synthesis

AuNPs of various sizes were synthesized as described by Frens.[30] For particles >10 nm, sodium citrate (Sigma-Aldrich, St Louis, Missouri) was employed, whereas sodium borohydride (Sigma-Aldrich) was used to generate particles of <10 nm. Briefly, 1 mL of 1% chloroauric acid (Sigma-Aldrich) was added to 90 mL ultrapurified water and quickly brought to a boil. Immediately upon rapid boiling, 0.4 to 1 mL of a 1% (wt/vol) sodium citrate solution was added to synthesize the various AuNP core sizes >10 nm. Similarly, 0.5 mL of 0.01 M chloroauric acid was added to 18 mL ultrapurified water, followed

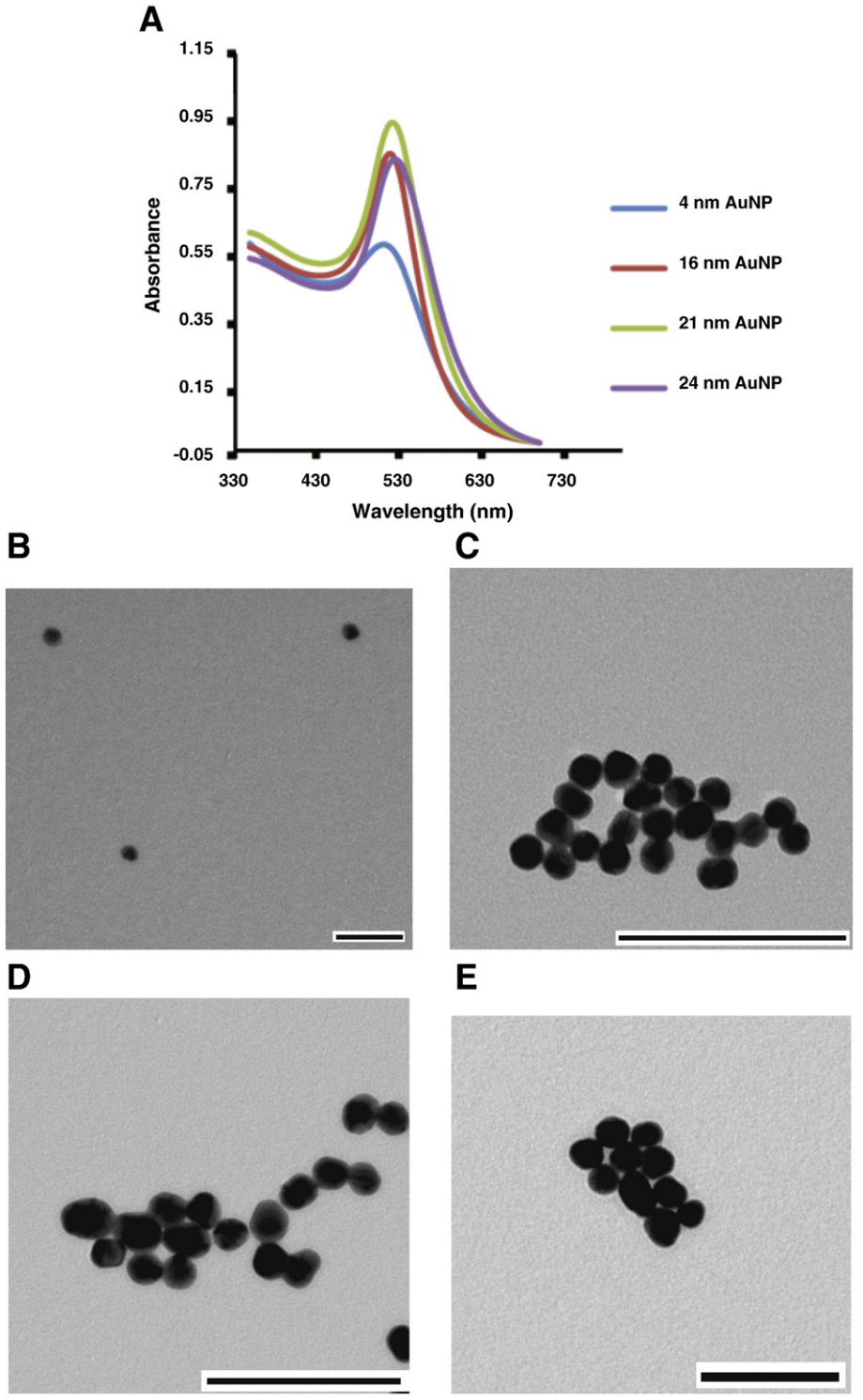

Figure 2. Characterization of AuNPs. **(A)** Ultraviolet-visible spectra of citrate-stabilized AuNPs of various core sizes with λ_{max} between 508 and 530 nm. **(B-E)** Transmission electron micrographs demonstrating spherical AuNPs with core sizes 4 nm, 16 nm, 21 nm, and 24 nm, respectively. The scale bar in *B* represents 20 nm; scale bars in *C-E* represent 100 nm.

by 0.5 mL of 0.01 M sodium citrate at room temperature while stirring for 5 minutes. To generate particles <10 nm, 0.4 to 1 mL of 0.1 M sodium borohydride was rapidly added to the above reaction mixture.

AuNP characterization

A UV-1601PC spectrophotometer (Shimadzu UV-1601PC; Shimadzu, Kyoto, Japan) was used to confirm the ultraviolet-

Table 1
TEM core sizes and corresponding hydrodynamic diameters

TEM core size (nm)	Hydrodynamic diameter (nm)
4	7
16	18
21	29
24	34

visible (UV-vis) absorption spectra of our particles. Hydrodynamic diameter (HD) and zeta potential of particles were then determined by dynamic light scattering using a Nano-ZS Zetasizer (Malvern Zetasizer Nano-ZS; Malvern Instruments, Worcestershire, United Kingdom). PEG-AuNPs were suspended in water, and zeta potential was measured at neutral pH. Transmission electron microscopy (TEM) was used for assessment of particle size. Briefly, samples were loaded onto carbon-coated copper grids, and images were obtained using Hitachi HD2000 STEM (Hitachi USA, Pleasanton, California). Particle sizes were measured from TEM using Image J software version 1.39 (National Institutes of Health, Bethesda, Maryland). Images were initially converted to 8-bit gray scale, and the scale was set appropriately. The imaging thresholds were then adjusted such that only particles were visualized on the image. The particle surface areas were then measured, and their respective diameters were computed from surface area measurements.

AuNP PEGylation

For PEGylation, a 1:5 molar ratio of thiolated PEG [molecular weight (MW) 1000, 2000, 5000, 10,000] to particle surface area was added to each AuNP synthesis while stirring at room temperature (25°C), and incubated 12 hours to generate PEG-AuNPs. PEG-AuNPs were collected by centrifugation at 18,000 *g* in an Avanti Series centrifuge (Beckman-Coulter, Brea, California). The pellet was washed with ultrapurified water, resuspended in 1 mL of medium, and filtered using a 0.22-μm syringe filter. Particles were stored at 4°C.

Particle stability

PEG-AuNPs and AuNPs were incubated in 1% (vol/vol) saline (room temperature) as well as in serum-free medium (37°C) overnight to assess stability. The particles were subsequently reanalyzed by UV-vis absorption spectroscopy to ascertain for any significant changes in absorption spectra. Particles were also evaluated for the presence of aggregates by light microscopy.

Construction of an in vitro brain microvasculature permeation model

To assess permeation of particles across endothelial cells, a well-described Transwell system (Corning Incorporated, Lowell, Massachusetts) was employed.[31-34] The system is made of an upper and lower chamber separated by a membrane with pore size 0.4 μm. Briefly, 1×10^5 RBECs were seeded on the upper membrane, and 5×10^4 RAs were seeded at the bottom portion of the membrane. Cells were grown until they were fully confluent, at which point the system was ready for transport testing (Figure 1).

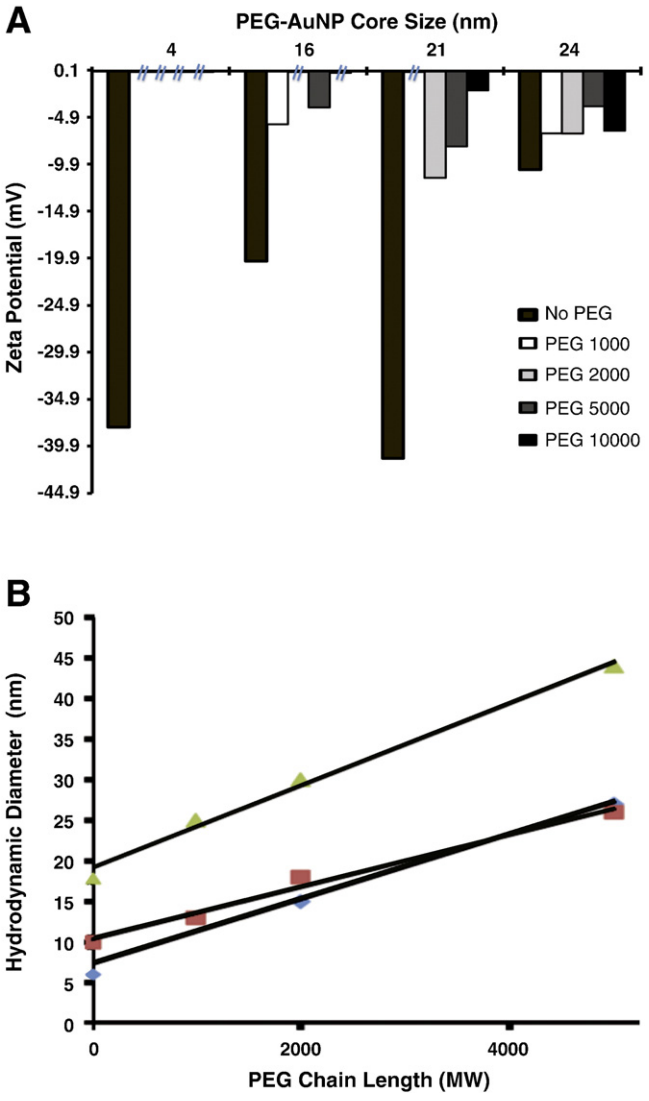

Figure 3. The effects of PEG surface chemistry on zeta potential and hydrodynamic diameter (HD). **(A)** PEG surface chemistry decreases the overall negative surface charge of citrate-stabilized AuNPs. Zeta potential values close to zero are demonstrated by double strikes through the *x*-axis. **(B)** Representative graph showing a linear relationship between PEG size and HD. Each line represents the effects of PEG size on the HD of a specific non-PEGylated AuNP.

Assessment of PEG-AuNP permeation

For transport assessment, PEG-AuNPs at various concentrations (700–5100 parts per billion) were introduced into the upper chamber with medium for 24 hours. Serum-supplemented media from both chambers were subsequently analyzed for gold content by inductively coupled plasma-atomic emission spectroscopy (Perkin Elmer Optima 3000 ICP AES; Perkin Elmer, Waltham, Massachusetts). Transport was ascertained from the relative

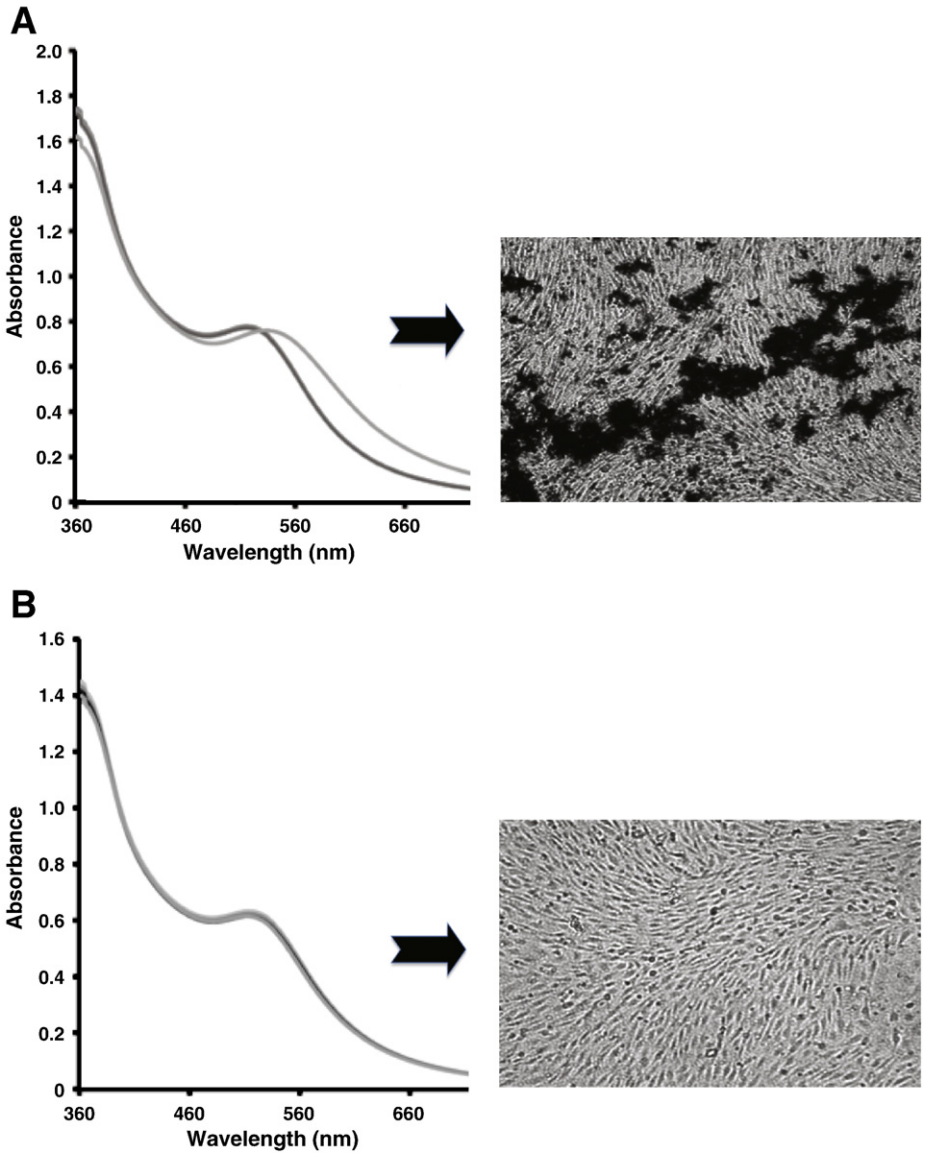

Figure 4. PEG surface chemistry confers stability and prevents aggregation of AuNPs in physiological solutions. **(A)** Absorption spectra data demonstrating a shift in absorbance when non-PEGylated AuNPs (4 nm) are incubated with 1% (vol/vol) saline (light graph) versus water (dark graph). Photomicrographs at 100× magnification demonstrate visible aggregates (black) of non-PEGylated AuNPs (4 nm) when incubated overnight at 37°C in serum-free medium within an endothelial cellular background. **(B)** Absorption spectra data demonstrating the absence of shift with PEG surface chemistry (4 nm coated with PEG 1000) when incubated in 1% (vol/vol) saline (light graph) versus water (dark graph) overnight at room temperature. Photomicrographs at 100× magnification demonstrate the absence of visible aggregates when AuNPs with PEG surface chemistry (4 nm coated with PEG 1000) are incubated in serum-free medium against endothelial cellular background.

content of gold in both chambers. Kinetic experiments were similarly performed using the smallest and largest particles with concentration ranges of 1900 to 8000 ppb. Chambers were sampled at 3 hours, 10 hours, and 20 hours, and analyzed for gold content as described above.

Statistics

Data were collected in at least triplicates. Analysis of variance was initially employed to identify differences between groups. Where differences were observed, Tukey's test was performed as a follow-up analysis for determination of statistical significance. Standard error of mean (SEM) values were employed in generating error bars. Statistical significance was based on $P < 0.05$.

Results

Synthesis and characterization of AuNPs

We synthesized AuNPs with HDs ranging from 6 to 34 nm based on the dynamic light scattering measurements. AuNPs

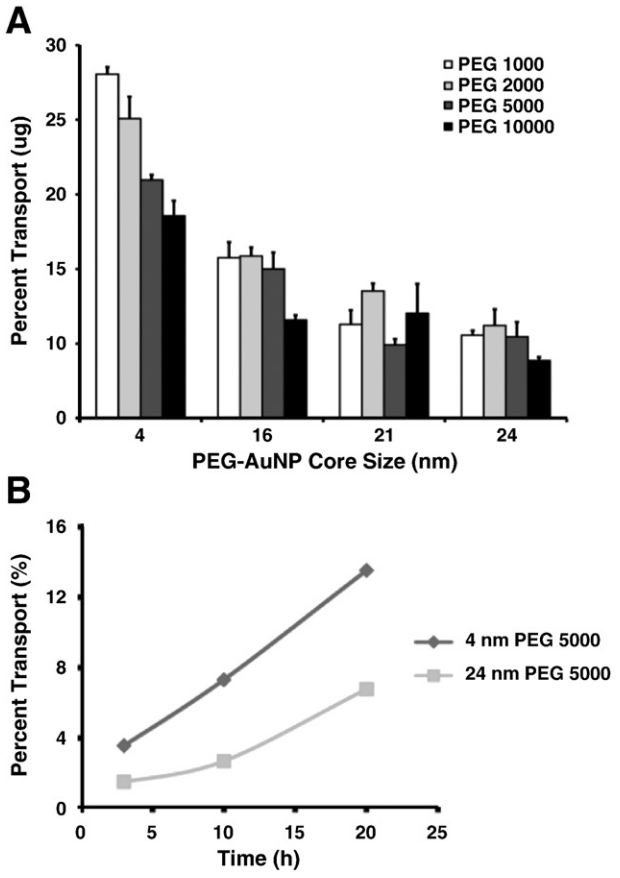

Figure 5. Permissive transport and kinetics of PEG-AuNPs across in vitro rat brain microvasculature model. **(A)** Bar graphs demonstrating a size-dependent transport profile of AuNPs of different PEG sizes as well as core sizes ($n = 3$, $P < 0.05$). **(B)** Line graph showing a faster and linear kinetic profile for the smallest core particle size 4 nm when compared to the largest core size 24 nm ($n = 3$, $P < 0.05$). Error bars represent SEM.

were synthesized by chemically reducing gold chloride[30] with sodium borohydride and citrate as previously described, to produce particles <10 nm, and >10 nm, respectively. When particles were further characterized by UV-vis spectrophotometry, we observed an absorption λ_{max} range from 508 to 530 nm. There was an increase in λ_{max} with increasing particle size (Figure 2, *A*). Particle core size was imaged by TEM analysis, which demonstrated spherical and well-dispersed NP populations (Figure 2, *B-E*). Based on TEM results, we selected the following AuNP sizes to conduct our studies: 4 nm, 16 nm, 21 nm, and 24 nm (Table 1)–all of which were within sizes previously reported to permeate brain endothelial cells following systemic administration.[28,29]

Design and characterization of PEG-AuNPs

Nonfunctionalized AuNPs have very limited clinical utility in vivo, because they tend to aggregate and demonstrate rapid clearance by the liver and spleen.[35-37] However, the coating of AuNPs with PEG surface chemistry circumvents several of these limitations. We therefore employed thiolated-PEG formulations of varying molecular weights (MW 1000, 2000, 5000, 10,000) based on optimization protocols from an earlier study.[27] UV-vis spectroscopy characterization of PEG-AuNPs demonstrated an increase in λ_{max}, which is characteristic of PEG functionality (Supplementary Figure S1, *A-D*, which can be found in the online version of this article). A linear correlation was noted between PEG size and HD for particles <20 nm (Figure 3, *B*). Incorporation of PEG functionality resulted in significant changes in the zeta potential from negative values to values closer to zero (Figure 3, *A*). Finally, PEG functionality was also noted to prevent aggregation and hence promote stability in saline as well as in serum-free culture medium (Figure 4, *A* and *B*). Aggregates of AuNPs were observed in medium when PEG functionality was absent. There were also changes in absorption spectra in the absence of PEG functionality. When incubated in 1% (vol/vol) saline, shifts in λ_{max} were noted.

Table 2
Permeation data for PEG-coated gold nanoparticles (AuNPs)

AuNP core size (nm)	PEG size (MW)	Permeation percent (± SEM)
4	1000	23.05 ± 0.47
4	2000	20.07 ± 1.47
4	5000	15.96 ± 0.35
4	10000	13.56 ± 1.01
16	1000	10.76 ± 1.03
16	2000	10.87 ± 0.57
16	5000	10.01 ± 1.10
16	10,000	6.59 ± 0.32
21	1000	6.30 ± 0.95
21	2000	8.52 ± 0.51
21	5000	4.92 ± 0.39
21	10,000	7.03 ± 1.20
24	1000	5.57 ± 0.31
24	2000	6.21 ± 1.09
24	5000	5.46 ± 0.98
24	10,000	3.86 ± 0.24

In vitro brain microvasculature permeation of PEG-AuNPs

Brain microvasculature permeation of PEG-AuNPs was assessed using a previously characterized model.[31-34] Our data (Figure 5, *A*) confirm a size-dependent transport of AuNPs with respect to both PEG-AuNP core size and PEG chain length. The mean percent permeation values and associated SEM data are listed (Table 2). Similarly, the statistical significance of permeation profiles between various PEG-AuNPs in terms of *P* values from the analysis of variance and Tukey analysis are listed in Table 3. Although all PEG-AuNPs sizes were noted to have brain microvasculature permeation, the most favorable transport profile was seen for the 4-nm PEG-AuNP size, which was statistically different in comparison to the other larger particles ($P < 0.01$). Moreover, a slightly favorable permeation profile was observed when low-MW PEG (1000, 2000) formulations of the 16-nm PEG-AuNPs were compared to PEG formulations of the 21-nm and 24-nm PEG-AuNPs ($P < 0.05$). There was no significant difference in permeation profiles between PEG formulations of the 21-nm and 24-nm PEG-AuNPs. The effect of PEG size on permeation was also appreciated. In general, whereas PEG formulation size appeared to be a more critical permeation determinant for the 4-nm AuNPs ($P < 0.01$), there was

Table 3
Statistical significance between PEG-AuNP permeation profiles from ANOVA and Tukey's test

PEG-AuNPs	4P1000	4P2000	4P5000	4P10,000	16P1000	16P2000	16P5000	16P10,000
4P1000	N.A.							
4P2000	N.S.	N.A.						
4P5000	$P < 0.01$	N.S.	N.A.					
4P10,000	$P < 0.01$	$P < 0.01$	N.S.	N.A.				
16P1000	$P < 0.01$	$P < 0.01$	$P < 0.01$	N.S.	N.A.			
16P2000	$P < 0.01$	$P < 0.01$	$P < 0.05$	N.S.	N.S.	N.A.		
16P5000	$P < 0.01$	$P < 0.01$	$P < 0.01$	N.S.	N.S.	N.S.	N.A.	
16P10,000	$P < 0.01$	$P < 0.01$	$P < 0.01$	$P < 0.01$	N.S.	N.S.	N.S.	N.A.
21P1000	$P < 0.01$	$P < 0.01$	$P < 0.01$	$P < 0.01$	$P < 0.05$	$P < 0.05$	N.S.	N.S.
21P2000	$P < 0.01$	$P < 0.01$	$P < 0.01$	$P < 0.05$	N.S.	N.S.	N.S.	N.S.
21P5000	$P < 0.01$	$P < 0.01$	$P < 0.01$	$P < 0.01$	$P < 0.01$	$P < 0.01$	$P < 0.05$	N.S.
21P10,000	$P < 0.01$	$P < 0.01$	$P < 0.01$	$P < 0.01$	N.S.	N.S.	N.S.	N.S.
24P1000	$P < 0.01$	$P < 0.01$	$P < 0.01$	$P < 0.01$	$P < 0.01$	$P < 0.01$	$P < 0.05$	N.S.
24P2000	$P < 0.01$	$P < 0.01$	$P < 0.01$	$P < 0.01$	$P < 0.05$	$P < 0.05$	N.S.	N.S.
24P5000	$P < 0.01$	$P < 0.01$	$P < 0.01$	$P < 0.01$	$P < 0.01$	$P < 0.01$	$P < 0.05$	N.S.
24P10,000	$P < 0.01$	$P < 0.01$	$P < 0.01$	$P < 0.01$	$P < 0.01$	$P < 0.01$	$P < 0.01$	N.S.

PEG-AuNPs	21P10,000	21P20,000	21P5000	21P10,000	24P1000	24P2000	24P5000	24P10,000
21P1000	N.A.							
21P2000	N.S.	N.A.						
21P5000	N.S.	N.S.	N.A.					
21P10,000	N.S.	N.S.	N.S.	N.A.				
24P1000	N.S.	N.S.	N.S.	N.S.	N.A.			
24P2000	N.S.	N.S.	N.S.	N.S.	N.S.	N.A.		
24P5000	N.S.	N.S.	N.S.	N.S.	N.S.	N.S.	N.A.	
24P10,000	N.S.	$P < 0.05$	N.S.	N.S.	N.S.	N.S.	N.S.	N.A.

ANOVA, analysis of variance; N.A., not applicable; N.S., not significant.

no significant effect on permeation of the other larger AuNPs. For AuNPs with core size of 4 nm, there were no significant permeation differences between PEG 1000 and PEG 2000 formulations. However, both the PEG 1000 and PEG 2000 formulations had superior permeation profiles in comparison to PEG 5000 and PEG 10,000 formulations for that particle size.

Finally, because we observed a size-dependent permeation of PEG-AuNPs, we were also interested in their respective kinetic profiles. Given that the most significant difference in transport was noted between the smallest particle (4 nm) and the other three particle sizes tested (16 nm, 21 nm, and 24 nm) as a group, we selected the 4-nm and 24-nm particles as surrogates for transport kinetics. Kinetics was assessed at 3 hours, 10 hours, and 20 hours using relative gold contents of the lower and upper Transwell chambers as indices of transport. The resulting kinetic profile was almost linear for the smaller particle in comparison to the larger particle (Figure 5, *B*). Moreover, the smaller particle (4 nm) had a steeper slope than larger particles, suggesting faster kinetics. This is in concordance with the permeation data. The linear kinetic profile appears to be consistent with a predominantly passive permeation process, although other associated active mechanisms cannot be entirely excluded.

Discussion

The current prognosis for patients with malignant brain tumors is very dismal. Similar to solid tumors, malignant brain tumors exhibit disorganized neovascularization with concomitant disruption of brain microvasculature integrity. The presence of a porous brain microvasculature around the tumor provides an avenue for selective permeation and passive accumulation of NPs through a phenomenon termed EPR.[1,2] Given substantial tumor-targeting potential of AuNPs for systemic cancers, as well the dire need for novel approaches to brain tumor targeting, the work presented here provides new insight into the contribution of the AuNP core and PEG surface functionality to brain microvasculature permeation.

AuNPs with various PEG sizes were employed in this study in light of the favorable biocompatibility attributes of PEG.[21-26] Furthermore, the selection of AuNP core sizes was based upon data from previous biodistribution studies, where particles of the specified core sizes had been shown to permeate the blood-brain interface.[28,29] In general, PEGylation of AuNPs resulted in slight increases in maximum absorption and overall particle stability when compared to non-PEG AuNPs. A linear correlation was noted between increases in NP HD with increases in PEG chain length. Given that we employed a linear PEG polymer, we hypothesize that the linear expansion of HD is most likely a function of PEG orientation on the surface of the NP. Based on this hypothesis, we would accordingly expect a linear orientation of PEG molecules on the surface of AuNPs, which would allow for a linear correlation between increases in PEG length and increases in particle size.

Another noteworthy consequence of PEG functionality was the significant change in the zeta potential from negative values to values closer to zero. This phenomenon was more pronounced for small NPs compared to large NPs, suggesting differential PEG surface coverage. Hence it would appear that smaller NPs

would be clinically advantageous and desirable in light of their efficient PEG coverage. Although it is unclear why this was the case, the observed reductions in surface negative charge were probably indicative of the replacement of citrate surface chemistry by PEG, because neutral PEG formulations were employed in our studies. In addition, because neutral PEG formulations were employed, our permeation data were most likely governed by AuNP size as opposed to charge. Finally, PEG functionality was also noted to prevent aggregation and hence promote stability in saline as well as in serum-free culture medium. In the absence of PEG functionality, AuNPs exhibited an absorbance shift in 1% (vol/vol) saline and a tendency to aggregate in medium, both of which would be undesirable properties for in vivo application. The actual permeation experiments were performed in serum-supplemented medium, which would have been more reflective of the in vivo scenario. Our study did not account for the potential effects of serum proteins on AuNP HD. However, we would anticipate a smaller effect given the presence of PEG coating.

The permeation of PEG-AuNPs within transport-permissive brain microvasculature is of paramount significance for brain tumor-targeting applications. Based on our model, there was a size-dependent permeation with respect to both NP core size as well as PEG chain length. Of all the core AuNP sizes tested, the 4-nm AuNPs had the most favorable transport and kinetic profile, suggesting that particles of such dimensions may be valuable for brain tumor-targeting applications. Although the remaining three AuNP core sizes (16 nm, 21 nm, and 24 nm) also demonstrated permeation through brain microvasculature cells, their respective permeation profiles were not substantially different from each other. These data suggest that when rat brain microvasculature cells are permissive to AuNP permeation, particle core size is a critical determinant. This is consistent with a prior in vivo study by a co-author, whereby size-dependent permeation of PEG-AuNPs was demonstrated in a breast tumor flank model.[27] Size-dependent transport appears to be a very consistent feature of NPs behavior within biological systems, especially with respect to cellular[38-40] and organ uptake.[28,29,41,42] Smaller NPs traditionally have higher permeations, which appear to be consistent with our findings here.

Furthermore, our study uncovers a novel finding with respect to PEG chain functionality. Our data suggest that the size contribution from PEG chain functionality is more of a critical permeation determinant for AuNPs with core sizes of ~4 nm. PEG chain size did not appear to significantly influence transport for AuNPs with core sizes >16 nm. A hypothesis for this observation may relate to the ratio of PEG length to particle core diameter. With increases in PEG length, one should expect this ratio to be significantly increased in smaller NPs compared to larger NPs. Therefore, within a size-dependent transport paradigm, increases in PEG length should preferentially influence transport in smaller particles as was observed here. Furthermore, the smaller MW PEG formulations (PEG 1000, PEG 2000) were more readily transported than their higher MW counterparts (PEG 5000, PEG 10,000). Thus, it would appear that particles within the 4-nm range would be most amenable to PEG chain size modifications for optimized permeation into the brain microvasculature.

Our data clearly do not address the issue of NP retention, which is an equally important aspect of targeted delivery. Such data can only be established in an in vivo setting. As previously demonstrated, permeation and retention appear to have an inverse correlation with respect to NP size.[27] Hence, whereas smaller NPs have higher permeations, their in vivo retention is not surprisingly low. Finally, our findings with respect to PEG polymeric chain size design could also have implications in the design of PEG-AuNPs suitable for targeting within the brain in other scenarios where the microvasculature is permissive to permeation such as in brain infections. In general, short PEG chain length (MW 1000-2000) in combination with smallest core size of 4 nm led to optimum permeation in our model system (Figure 6).

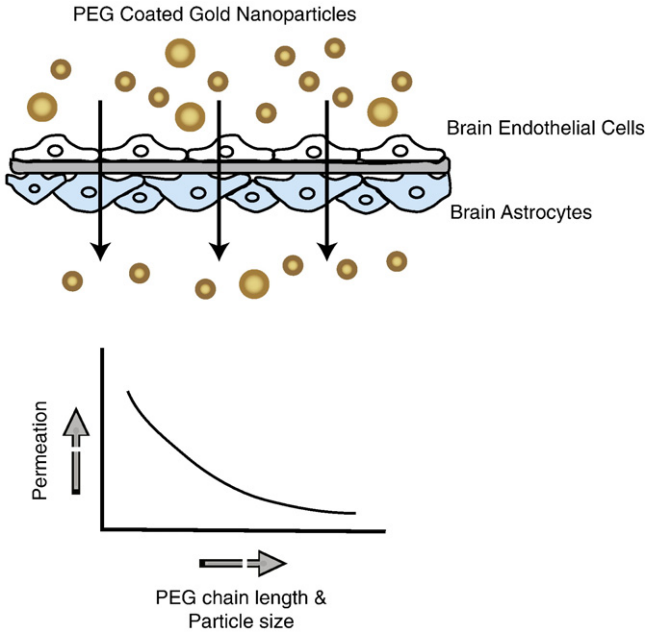

Figure 6. Brain microvasculature permeation model–the influence of PEG size design on AuNP permeation. Model of brain microvasculature cells whereby short PEG chain length (MW 1000–2000) in combination with small core size exhibit optimum permeation.

In summary, our study provides insights on the effects of PEG chain size design on PEG-AuNP permeation in the brain microvasculature using an in vitro platform. Although our assessment was done in vitro, we hypothesize that the relative permeations observed would be similar in an in vivo system that is permissive to PEG-AuNP permeation. Furthermore, our data are consistent with the previous in vivo tumor permeation study outside the central nervous system[27] using a similar NP platform. Future studies will entail assessment of PEG-AuNP permeation in murine orthotopic human brain tumor xenografts following intravenous as well as intra-arterial deliveries.

Appendix A. Supplementary data

Supplementary materials related to this article can be foundonline at doi:10.1016/j.nano.2011.04.004.

References

1. Maeda H. The enhanced permeability and retention (EPR) effect in tumor vasculature: the key role of tumor-selective macromolecular drug targeting. Adv Enzyme Regul 2001;41:189-207.

2. Greish K. Enhanced permeability and retention of macromolecular drugs in solid tumors: a royal gate for targeted anticancer nanomedicines. J Drug Target 2007;15:457-64.
3. Schneider SW, Ludwig T, Tatenhorst L, Braune S, Oberleithner H, Senner V, et al. Glioblastoma cells release factors that disrupt blood-brain barrier features. Acta Neuropathol 2004;107:272-6.
4. Criscuolo GR. The genesis of peritumoral vasogenic brain edema and tumor cysts: a hypothetical role for tumor-derived vascular permeability factor. Yale J Biol Med 1993;66:277-314.
5. Strugar J, Rothbart D, Harrington W, Criscuolo GR. Vascular permeability factor in brain metastases: correlation with vasogenic brain edema and tumor angiogenesis. J Neurosurg 1994;81:560-6.
6. Gerstner ER, Duda DG, di Tomaso E, Ryg PA, Loeffler JS, Sorensen AG, et al. VEGF inhibitors in the treatment of cerebral edema in patients with brain cancer. Nat Rev Clin Oncol 2009;6:229-36.
7. Stummer W. Mechanisms of tumor-related brain edema. Neurosurg Focus 2007;22:E8.
8. Connor EE, Mwamuka J, Gole A, Murphy CJ, Wyatt MD. Gold nanoparticles are taken up by human cells but do not cause acute cytotoxicity. Small 2005;1:325-7.
9. Male KB, Lachance B, Hrapovic S, Sunahara G, Luong JH. Assessment of cytotoxicity of quantum dots and gold nanoparticles using cell-based impedance spectroscopy. Anal Chem 2008;80:5487-93.
10. Paciotti GF, Myer L, Weinreich D, Goia D, Pavel N, McLaughlin RE, et al. Colloidal gold: a novel nanoparticle vector for tumor directed drug delivery. Drug Deliv 2004;11:169-83.
11. Hainfeld JF, Slatkin DN, Smilowitz HM. The use of gold nanoparticles to enhance radiotherapy in mice. Phys Med Biol 2004;49:N309-15.
12. Mukherjee P, Bhattacharya R, Wang P, Wang L, Basu S, Nagy JA, et al. Antiangiogenic properties of gold nanoparticles. Clin Cancer Res 2005;11:3530-4.
13. Brown SD, Nativo P, Smith JA, Stirling D, Edwards PR, Venugopal B, et al. Gold nanoparticles for the improved anticancer drug delivery of the active component of oxaliplatin. J Am Chem Soc 2010;132: 4678-84.
14. Cheng Y, Samia A, Meyers JD, Panagopoulos I, Fei B, Burda C. Highly efficient drug delivery with gold nanoparticle vectors for in vivo photodynamic therapy of cancer. J Am Chem Soc 2008;130: 10643-7.
15. Hirsch LR, Stafford RJ, Bankson JA, Sershen SR, Rivera B, Price RE, et al. Nanoshell-mediated near-infrared thermal therapy of tumors under magnetic resonance guidance. Proc Natl Acad Sci U S A 2003;100: 13549-54.
16. Visaria RK, Griffin RJ, Williams BW, Ebbini ES, Paciotti GF, Song CW, et al. Enhancement of tumor thermal therapy using gold nanoparticle-assisted tumor necrosis factor-alpha delivery. Mol Cancer Ther 2006; 5:1014-20.
17. Huang X, Jain PK, El-Sayed IH, El-Sayed MA. Plasmonic photothermal therapy (PPTT) using gold nanoparticles. Lasers Med Sci 2008;23: 217-28.
18. Bernardi RJ, Lowery AR, Thompson PA, Blaney SM, West JL. Immunonanoshells for targeted photothermal ablation in medulloblastoma and glioma: an in vitro evaluation using human cell lines. J Neurooncol 2008;86:165-72.
19. Schwartz JA, Shetty AM, Price RE, Stafford RJ, Wang JC, Uthamanthil RK, et al. Feasibility study of particle-assisted laser ablation of brain tumors in orthotopic canine model. Cancer Res 2009;69:1659-67.
20. Libutti SK, Paciotti GF, Byrnes AA, Alexander Jr HR, Gannon WE, Walker M, et al. Phase I and pharmacokinetic studies of CYT-6091, a novel PEGylated colloidal gold-rhTNF nanomedicine. Clin Cancer Res 2010;16:6139-49.
21. Veiseh O, Sun C, Gunn J, Kohler N, Gabikian P, Lee D, et al. Optical and MRI multifunctional nanoprobe for targeting gliomas. Nano Lett 2005;5:1003-8.
22. Kohler N, Fryxell GE, Zhang M. A bifunctional poly(ethylene glycol) silane immobilized on metallic oxide-based nanoparticles for conjugation with cell targeting agents. J Am Chem Soc 2004;126:7206-11.
23. Cai W, Shin DW, Chen K, Gheysens O, Cao Q, Wang SX, et al. Peptide-labeled near-infrared quantum dots for imaging tumor vasculature in living subjects. Nano Lett 2006;6:669-76.
24. Susumu K, Uyeda HT, Medintz IL, Pons T, Delehanty JB, Mattoussi H. Enhancing the stability and biological functionalities of quantum dots via compact multifunctional ligands. J Am Chem Soc 2007;129:13987-96.
25. Liu Z, Winters M, Holodniy M. Dai H. siRNA delivery into human T cells and primary cells with carbon-nanotube transporters. Angew Chem Int Edn Engl 2007;46:2023-7.
26. Dixit V, Van den Bossche J, Sherman DM, Thompson DH, Andres RP. Synthesis and grafting of thioctic acid-PEG-folate conjugates onto Au nanoparticles for selective targeting of folate receptor-positive tumor cells. Bioconjug Chem 2006;17:603-9.
27. Perrault SD, Walkey C, Jennings T, Fischer HC, Chan WC. Mediating tumor targeting efficiency of nanoparticles through design. Nano Lett 2009;9:1909-15.
28. Sonavane G, Tomoda K, Makino K. Biodistribution of colloidal gold nanoparticles after intravenous administration: effect of particle size. Colloids Surf B Biointerfaces 2008;66:274-80.
29. De Jong WH, Hagens WI, Krystek P, Burger MC, Sips AJ, Geertsma RE. Particle size-dependent organ distribution of gold nanoparticles after intravenous administration. Biomaterials 2008;29:1912-9.
30. Frens G. Controlled nucleation for the regulation of the particle size in monodisperse gold suspensions. Nature 1973;241:20-2.
31. Garberg P, Ball M, Borg N, Cecchelli R, Fenart L, Hurst RD, et al. In vitro models for the blood-brain barrier. Toxicol in Vitro 2005;19: 299-334.
32. Culot M, Lundquist S, Vanuxeem D, Nion S, Landry C, Delplace Y, et al. An in vitro blood-brain barrier model for high throughput (HTS) toxicological screening. Toxicol in Vitro 2008;22:799-811.
33. Stanness KA, Westrum LE, Fornaciari E, Mascagni P, Nelson JA, Stenglein SG, et al. Morphological and functional characterization of an in vitro blood-brain barrier model. Brain Res 1997;771:329-42.
34. Nakagawa S, Deli MA, Kawaguchi H, Shimizudani T, Shimono T, Kittel A, et al. A new blood-brain barrier model using primary rat brain endothelial cells, pericytes and astrocytes. Neurochem Int 2009;54: 253-63.
35. Romberg B, Hennink WE, Storm G. Sheddable coatings for long-circulating nanoparticles. Pharm Res 2008;25:55-71.
36. Moghimi SM, Hunter AC, Murray JC. Long-circulating and target-specific nanoparticles: theory to practice. Pharmacol Rev 2001;53: 283-318.
37. Owens III DE, Peppas NA. Opsonization, biodistribution, and pharmacokinetics of polymeric nanoparticles. Int J Pharm 2006;307: 93-102.
38. Alkilany AM, Nagaria PK, Hexel CR, Shaw TJ, Murphy CJ, Wyatt MD. Cellular uptake and cytotoxicity of gold nanorods: molecular origin of cytotoxicity and surface effects. Small 2009;5:701-8.
39. Chithrani BD, Chan WC. Elucidating the mechanism of cellular uptake and removal of protein-coated gold nanoparticles of different sizes and shapes. Nano Lett 2007;7:1542-50.
40. Chithrani BD, Ghazani AA, Chan WC. Determining the size and shape dependence of gold nanoparticle uptake into mammalian cells. Nano Lett 2006;6:662-8.
41. Semmler-Behnke M, Kreyling WG, Lipka J, Fertsch S, Wenk A, Takenaka S, et al. Biodistribution of 1.4- and 18-nm gold particles in rats. Small 2008;4:2108-11.
42. Terentyuk GS, Maslyakova GN, Suleymanova LV, Khlebtsov BN, Kogan BY, Akchurin GG, et al. Circulation and distribution of gold nanoparticles and induced alterations of tissue morphology at intravenous particle delivery. J Biophotonics 2009;2:292-302.